Ocean Engineering 266 (2022) 112621

Contents lists available at ScienceDirect

Ocean Engineering

journal homepage: www.elsevier.com/locate/oceaneng

Fatigue reliability of mooring chains, including mean load and corrosion effects

Erling N. Lone [a,*], Thomas Sauder [b,a], Kjell Larsen [a,c], Bernt J. Leira [a]

[a] Department of Marine Technology, Norwegian University of Science and Technology, Trondheim N-7491, Norway
[b] SINTEF Ocean, P.O. Box 4762 Torgarden, 7465 Trondheim, Norway
[c] Equinor ASA, Arkitekt Ebbells veg 10, 7053 Ranheim, Norway

ARTICLE INFO

Keywords:
Studless chain
S-N approach
Sensitivity analysis
Reliability analysis
Mean load
Corrosion

ABSTRACT

A reliability formulation for mooring chain fatigue is developed, including the effects of mean load and degradation due to corrosion. They are included by starting from a S-N model with parameterized dependence to the mean load and a customized corrosion condition scale. The paper includes a thorough case study, based on a realistic case. A global sensitivity analysis is used to justify a reduction of the model dimension. A reliability analysis is then performed, and the effect on failure probability from variation of a range of parameters and model assumptions is studied.

1. Introduction

Fatigue assessment of offshore mooring systems is required by relevant rules and standards (ISO 19901-7, 2013; DNV GL, 2018), to demonstrate satisfactory resistance towards exposure to cyclic loads. These fatigue calculations are subject to considerable uncertainties with respect to both loads and capacity, requiring fatigue safety factors typically ranging from 5 to 8 (DNV GL, 2018). These fairly large safety factors aim to satisfy a maximum annual probability of mooring line failure in the range from 10^{-3} to 10^{-5} (DNV GL, 2018; Mathisen et al., 1999; Mathisen and Hørte, 2005). Nevertheless, mooring lines tend to fail at a much higher rate (Ma et al., 2013; Kvitrud, 2014; Fontaine et al., 2014). The root causes are diverse, however; almost half of the events described in Fontaine et al. (2014) were related to chain components and almost half of those were caused by fatigue and corrosion. Likely contributors to these failures are uncertainties in dynamic loads and a lack of proper models to account for effects governing the fatigue capacity of mooring chains.

The fatigue capacity curves prescribed by current design codes (ISO 19901-7, 2013; DNV GL, 2018) are based on fatigue tests of new chain performed at a mean load of 20% of the minimum breaking load (MBL) (Gabrielsen et al., 2019). In the fatigue calculations, the actual mean loads of the mooring lines are disregarded, whereas degradation due to corrosion is accounted for in a simplified manner by reducing the cross section area of the chains, giving an increase in the effective stress ranges entering the calculations. However, full scale fatigue tests performed in recent years for both new and used studless mooring chains have revealed that (i) the fatigue capacity of chains is strongly dependent on the mean load, and (ii) realistic corrosion pits have a detrimental effect not well represented by the simplified approach prescribed by the standards (Gabrielsen et al., 2019; Fernández et al., 2019; Zhang and Smedley, 2019; Ma et al., 2019; Lone et al., 2021). Hence, proper treatment of mean load effect and degradation due to corrosion in the calculations seems imperative to enable improved estimation of mooring line fatigue life.

The effects of mean load and corrosion on fatigue of mooring chain have been addressed previously. Martinez Perez et al. (2018, 2019) presented a computational method that accounts for the influence of mean load on the fatigue lifetime of new mooring chain. Zarandi and Skallerud (2020) investigated the effect of mean load including residual stresses on the fatigue crack initiation of corroded chains using experiments and finite element analysis. Lardier et al. (2008) used a fracture mechanics approach to address the combined effect of fatigue cracks and material loss due to corrosion on the fatigue reliability of mooring chains. Wang et al. (2019) assessed the effect of location and geometry of corrosion pits on mooring chain fatigue life using finite element analysis. Mendoza et al. (2022) presented the effect of pitting corrosion on the fatigue reliability of a chain link. None of these do, however, consider the combined effect of mean load and corrosion on the fatigue reliability of mooring chain.

Based on test results for new and used chain, tested at a range of mean load levels and with various degrees of corrosion, Lone et al. (2021) established a fatigue capacity model with parameterized dependence to mean load and a customized corrosion measure. This work

* Corresponding author.
E-mail addresses: erling.lone@ntnu.no (E.N. Lone), thomas.sauder@sintef.no (T. Sauder), kjell.larsen@ntnu.no (K. Larsen), bernt.leira@ntnu.no (B.J. Leira).

https://doi.org/10.1016/j.oceaneng.2022.112621
Received 6 May 2022; Received in revised form 1 September 2022; Accepted 15 September 2022
Available online 10 October 2022

Nomenclature

X_i	ith component of random vector $\boldsymbol{X}$
E[·]	Mathematical expectation
P[·]	Probability measure
Var[·]	Variance
$\|\cdot\|$	Vector norm
ln(·)	Natural logarithm
log(·)	Common logarithm
$\sim$	distributed as
$LN(\mu,\sigma)$	Lognormal distribution with scale parameter $\exp\{\mu\}$ and shape parameter σ
$N(\mu,\sigma^2)$	Normal distribution with mean μ and variance σ^2
$U(a,b)$	Uniform distribution with support $[a,b]$
$\mathbb{R}_+$	Real numbers greater than or equal to zero
α_i	FORM importance factor, see (D.3)
β	FORM reliability index
ϵ	Regression error, see (3)
μ	Logarithm of scale parameter of lognormal distribution Mean value
σ	Shape parameter of lognormal distribution Standard deviation
σ_m	Mean stress [MPa]
$A(\sigma_m,c)$	Mean load and corrosion dependent intercept parameter of S-N curve, see (2)
B_0	Coefficient of S-N curve intercept parameter, see (2)
B_1	Coefficient of S-N curve intercept parameter (mean load effect), see (2)
B_2	Coefficient of S-N curve intercept parameter (corrosion grade effect), see (2)
c	Corrosion grade, support $[1,7]$
C_{end}	Corrosion grade at end of service life
D	Fatigue damage (Palmgren–Miner sum)
D_W	Fatigue damage of weakest link in a segment, see (9)
D_{cr}	Critical fatigue damage, i.e., Miner's sum at failure
$g(\boldsymbol{X};N_y,N)$	Limit state function for fatigue failure after N_y years for chain segment with N links
$g_1(\sigma_m)$	Mean load function, see (2)
G_1^*	Representative value of mean load function over a specified period, see (6)
$g_2(c)$	Corrosion grade function, see (2)
G_2^*	Representative value of corrosion grade function over a specified period
k	Index for year, for $k\in\{1,2,\dots,N_y\}$
M	Dimension of random vector
m	Slope parameter of S-N curve
N	Number of cycles to failure, see (1), or Number of links in the chain segment, see (10)
N_y	Number of years
$p_f^{(N)}$	Probability of failure for segment with N links, see (11)
Q_s,Q_m,Q_c	Model uncertainties for stress ranges, mean loads and corrosion grade, respectively, see Section 3.2
S	Stress range [MPa]
S_i	First-order Sobol' index, see (D.1)
S_{Ti}	Total effect Sobol' index, see (D.2)
W	Deviation from median fatigue capacity for weakest link in a segment, see (10)
Z	Fatigue load, see (4)
CoV	Coefficient of Variation
FORM	First Order Reliability Method
i.i.d.	independent and identically distributed
IS	Importance Sampling
MBL	Minimum Breaking Load
MCS	Monte Carlo Simulation

formed the basis for a probabilistic fatigue damage model, presented in Lone et al. (2022) and briefly summarized in Section 2. In the present paper, we present a formulation of fatigue reliability for mooring chain segments that for the first time accounts properly for mean load and corrosion effects.

The paper is organized as follows. In Section 2, we review the mean load and corrosion dependent fatigue capacity model and the probabilistic fatigue damage model. In Section 3, we develop the reliability formulation for fatigue failure of mooring chain segments including the effects of mean load and corrosion condition. In Section 4, some additional aspects of the reliability formulation are discussed. In Section 5, we apply the reliability formulation to a case study to discuss relevant assumptions and properties of the fatigue reliability model. Conclusions are given in Section 6.

2. Background: Probabilistic fatigue model

In this section, we review the mean load and corrosion dependent fatigue capacity model presented in Lone et al. (2021) and the probabilistic fatigue damage model proposed in Lone et al. (2022) in the context of the present paper. We apply the usual convention of describing random variables by capital letters (e.g., X), small letters to describe a realization of a random variable (e.g., x), and bold symbols to denote vectors or matrices (e.g., $\boldsymbol{X},\boldsymbol{x}$).

2.1. Mean load and corrosion dependent fatigue capacity

The S-N approach to fatigue of mooring chain is considered. Fatigue capacity is then expressed in terms of a stress-life (S-N) curve, defined as

$$N\cdot S^m = A \tag{1}$$

where N is the number of cycles to failure at constant stress range S, m is the slope parameter and A is referred to as the intercept parameter. To account for the effect of mean load and corrosion on the fatigue capacity, Lone et al. (2021) expressed the intercept parameter as function of these parameters:

$$\log A(\sigma_m,c) = B_0 + B_1\cdot g_1(\sigma_m) + B_2\cdot g_2(c) \tag{2}$$

where log(·) is the common logarithm, $(B_j)_{j\in\{0,1,2\}}$ are coefficients and $g_1(\sigma_m)$ and $g_2(c)$ are monotonically increasing functions of the mean stress σ_m and a corrosion grade c, respectively. The corrosion grade applied here is based on a customized scale ranging from 1 (new chain or mild corrosion) to 7 (severe corrosion), see Lone et al. (2021) for details.

The first term in (2) describes the constant (time-invariant) part of the fatigue capacity. The second term describes the mean load effect; a negative value of B_1 implies that the fatigue capacity increases when the mean load is reduced. The last term describes the deteriorating effect of corrosion; a negative value of B_2 implies that the fatigue capacity is reduced when the corrosion grade increases.

The coefficients of the mean load and corrosion dependent S-N model were estimated empirically from a database of full scale fatigue tests, by considering the regression model

$$\begin{aligned}\log N_i &= B_0 + B_1\cdot g_1(\sigma_{m,i}) + B_2\cdot g_2(c_i) - m\cdot\log S_i + \epsilon_i\\ \epsilon_i &\sim N(0,\sigma_\epsilon^2)\end{aligned} \tag{3}$$

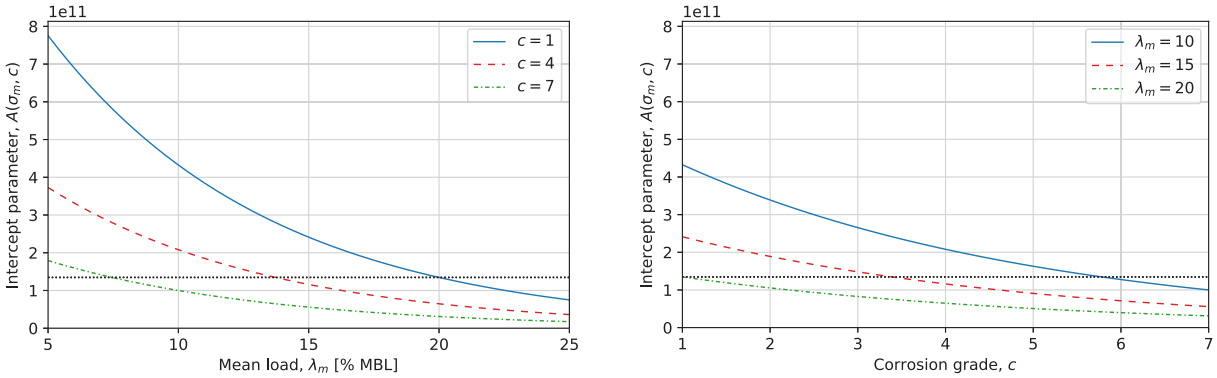

Fig. 1. S-N curve intercept parameter fitted to fatigue tests of used and new chains (Lone et al., 2021), as function of mean load (left) and corrosion grade (right). The horizontal dotted line is located at a reference value $A = 1.346 \times 10^{11}$ ($\log A = 11.129$) corresponding to $\lambda_m = 20$ [% MBL] and $c = 1$.

Table 1
S-N curve parameters estimated by least-squares regression with $m = 3$, from fatigue tests of used and new studless chains (Lone et al., 2021).

$g_1(\sigma_m)$	$g_2(c)$	$\hat{B}_0$	$\hat{B}_1$	$\hat{B}_2$	$\hat{\sigma}_\epsilon$
λ_m	c	12.249	−0.0507	−0.106	0.17

with the stress range effect fixed at $m = 3$. Here, the subscript i is a counter for fatigue test samples and ϵ is the regression error representing the predictive uncertainty of the regression model, see e.g., Gelman and Hill (2007).

In total the database consisted of 125 samples of studless chain, tested at various mean loads and for various degrees of corrosion; 77 tests for used chains retrieved after operation in the North Sea, and 48 tests for new chains. The most adequate mean load function was found to be $g_2(\sigma_m) = \lambda_m$, where λ_m is the mean load expressed in percentage of the minimum breaking load (MBL). For corrosion grade, the best fit to data was achieved with $g_2(c) = c$. S-N model parameters obtained from least-squares regression in Lone et al. (2021) are listed in Table 1, and the corresponding intercept parameter is visualized in Fig. 1 for various values of the mean load and corrosion grade.

We will retain the generic notation $g_1(\cdot)$ and $g_2(\cdot)$ in the subsequent section for the sake of generality.

2.2. Probabilistic fatigue damage

The following assumptions are made:

- The Palmgren–Miner hypothesis on linear accumulation of the fatigue effect from each stress cycle is adopted for variable amplitude loading.
- The S-N curve slope parameter (stress range effect, m) is assumed fixed.
- Time-variant random variables may be considered as piecewise time-invariant.

We introduce a *fatigue load* variable as

$$Z = n_0 \cdot \mathrm{E}[S^m] \tag{4}$$

where n_0 is the number of stress cycles and $\mathrm{E}[S^m]$ is the mth moment of the stress range distribution for a given time period. By application of Miner's rule, the fatigue damage after N_y years may then be expressed as a summation over annual contributions (Lone et al., 2022):

$$D(\boldsymbol{X}; N_y) = \sum_{k=1}^{N_y} \frac{Z_k}{10^{\left(B_0 + B_1 \cdot G^*_{1,k} + B_2 \cdot G^*_{2,k} + \epsilon\right)}} \tag{5}$$

where $\boldsymbol{X} = (B_0, B_1, B_2, \epsilon, \boldsymbol{Z}, \boldsymbol{G}^*_1, \boldsymbol{G}^*_2)$ contains the underlying random variables, k is a counter for years, and $G^*_{1,k}$ and $G^*_{2,k}$ are representative values of the mean load and the corrosion grade functions in the kth year, respectively. Note that in Lone et al. (2022), the uncertainty associated with the S-N model error (ϵ) was included in the uncertainty of B_0. Here, we choose to express this uncertainty explicitly, for reasons that will become clear in Section 3.

This fatigue damage model in (5) enables accounting for both prior, known loads and future, uncertain loads. Hence, the vector $\boldsymbol{Z}$, containing fatigue loads for each of the N_y years, may consist of both deterministic and random quantities. For instance; if the damage is estimated for N_p prior years and N_f future years, we have $\boldsymbol{Z} = (z_1, \ldots, z_{N_p}, Z_{N_y - N_f + 1}, \ldots, Z_{N_y})$. That is, $\boldsymbol{Z}$ then consists of N_p deterministic quantities and N_f random quantities.

The mean load and corrosion dependent intercept parameter in (2) introduces a time-dependency to the fatigue capacity, which varies both over years and during the course of each year due to mean load variations and the temporal corrosion development. The annual variations are accounted for by allowing the values of G^*_1 and G^*_2 to vary by year in Eq. (5). By introducing representative values for the mean load and corrosion grade functions, we ensure that the piecewise time-invariant summation accounts properly also for the within-year variations.

The vector of representative mean load values ($\boldsymbol{G}^*_1$) is constructed in a way similar to that of the fatigue loads. For the N_p prior years with known load history, the representative mean load values are calculated deterministically from the joint, empirical distributions of mean loads and stress ranges for each year (Lone et al., 2022):

$$g^*_{1,k} = -\frac{1}{b_1} \log\left[\frac{\sum_i n_i \cdot s_i^m \cdot 10^{-b_1 \cdot g_1(\sigma_{m,i})}}{n_{0,k} \cdot \mathrm{E}[S^m]_k}\right] \tag{6}$$

where index i refers to tuples with $(n_i, s_i, \sigma_{m,i})$ from a joint histogram of stress ranges and mean stress: n_i is the number of joint occurrences of stress range s_i and mean stress $\sigma_{m,i}$, $n_{0,k} = \sum_i n_i$ is the total number of stress cycles, $\mathrm{E}[S^m]_k = \frac{1}{n_{0,k}} \sum_i n_i \cdot s_i^m$ is the mth moment of the stress range distribution, and all summations are over observations in the kth year. In this calculation, the mean load coefficient B_1 is assumed fixed at a given value b_1. Appendix A.1 shows that the representative mean load calculated from (6) is typically insensitive to variations in the mean load coefficient.

For the N_f future years, the representative mean load is generally represented by stochastic quantities. A fixed value for future years may however be justified if the annual variability is found to be sufficiently low, or if the effect of annual variability on the quantity of interest is shown to be negligible. Note that results presented in Lone et al. (2022) showed that the representative mean load may be correlated with the annual fatigue load. Alternative ways to address this correlation are discussed in Section 4.

Unlike the fatigue load and representative mean load, the corrosion grade may be subject to uncertainty for both prior and future years.

This may be the case even if inspections are performed, since the categorization from inspection is subject to some uncertainty, and inspections yield corrosion grade estimates for those specific times but not for the intermediate time periods. Hence, in the case of chain inspections, the construction of $\boldsymbol{G}_2^*$ must be based on an assessment of the quality and uncertainty of the inspections, as well as the uncertainty of the intermediate and future states. On the other hand, if nothing is known about the corrosion state of the chains it may be convenient to let $\boldsymbol{G}_2^*$ be a function of some underlying random variable(s), such as for instance the corrosion grade at the end of the service life and some parameter that describes the shape of its temporal development. An example of such a model is presented in Lone et al. (2022).

In summary, the fatigue damage model in Eq. (5) represents an adaption of Miner's rule for damage accumulation that enables accounting for (i) the annual fatigue load variability, (ii) the effect on fatigue capacity from mean load (including time dependent variations) and degradation due to corrosion, and (iii) possible interactions between these. This forms the basis for the mooring chain reliability formulation that is developed in the next section.

3. Reliability formulation

For a deterministic case, fatigue failure is assumed to occur when the fatigue damage D reaches unity. In practice, Miner's rule is imperfect and subject to considerable uncertainty. Wirsching (1984) therefore argued that a more appropriate failure criterion is $D \geq D_{\text{cr}}$, where $D_{\text{cr}} \in \mathbb{R}_+$ is a random variable denoting the "critical" damage (i.e., the Miner's sum at failure). The probability of failure for a single chain *link* may then be expressed as

$$p_f^{(1)} = \mathrm{P}\left[D_{\text{cr}} \leq D(\boldsymbol{X}; N_y)\right] \tag{7}$$

where superscript $\cdot^{(1)}$ indicates that the failure event is for *one* link.

3.1. Failure of chain segment

A chain *segment* is here defined as a continuous mooring line section, composed of identical chain links. It constitutes a series system where failure of a single component leads to segment failure. Hence, the segment failure probability may be considerably over- or underestimated if partial dependence between the individual links is ignored or mistreated.[1]

As done in Larsen and Mathisen (1996), we account for the partial correlation by distinguishing the *variables* that are fully correlated between links from those that may be assumed to be independent. We assume that the following variables and properties are the *same* between links:

- $\boldsymbol{Z}$ (fatigue loads). This is considered a reasonable and realistic assumption, as links within a chain segment will indeed be exposed to very similar *dynamic* loads (hence, similar stress range distributions). Any deviations in the loads within a segment are assumed to be of minor importance.
- $\boldsymbol{G}_1^*$ (mean loads). Analogously, the mean loads are assumed to be the same for links within a segment. This is a slightly less accurate assumption, since the mean load in a catenary line will generally decrease with increasing distance from the fairlead in direction of the anchor.[2] Nevertheless, the mean loads within a segment will be practically fully correlated, and conservatism may be ensured by using the highest mean load within the segment (link closest to the fairlead).
- $\boldsymbol{G}_2^*$ (corrosion grades). Some variation of the corrosion grade would be expected along a segment, depending on segment length, location (position in water column, sea bed contact, etc.) and due to the inherent variability of the corrosion process. The need for a model addressing its spatial variation could therefore be justified. Here, we simplify the problem by assuming that the same corrosion grade applies to the entire segment. Conservatism may then be ensured by considering the most severe corrosion grade along the segment length as representative for all links. In the case that inspections reveal a systematic variation from one end of the segment to the other, this could be addressed by modeling the segment as two or more separate segments with different values for the corrosion grade.
- B_0, B_1, B_2 (S-N model parameters). This implies that the mean load and corrosion grade effects are assumed to be the same, and consequently, that the *median* fatigue capacity is the same for each link. This is consistent with the regression model in Eq. (3).
- D_{cr} (Miner's sum at failure). According to Lotsberg (2016, p. 115), the accuracy of Miner's rule is related to the shape of the fatigue load spectra. Hence, following the above assumption of similar fatigue loads, it is reasonable to assume the same Miner's sum at failure for links within a segment.

On the other hand, we assume that the *deviation* from the median fatigue capacity, expressed in terms of the S-N model error (ϵ), is independent and identically distributed (i.i.d.) for each link. Again, this assumption is consistent with the regression model in Eq. (3).

The fatigue damage of the ith component may then be expressed as:

$$D_i(\boldsymbol{X}_i; N_y) = \frac{1}{R_i} \sum_{k=1}^{N_y} \frac{Z_k}{10^{\left(B_0 + B_1 \cdot G_{1,k}^* + B_2 \cdot G_{2,k}^*\right)}} \tag{8}$$

where $R_i = 10^{\epsilon_i}$ denotes the deviation from median fatigue capacity, given the mean load and corrosion condition. The vector of random variables $\boldsymbol{X}_i$ now contains one independent variable (R_i), whereas the remaining variables take on the same value for all links ($B_0, B_1, B_2, \boldsymbol{Z}, \boldsymbol{G}_1^*, \boldsymbol{G}_2^*$). We now define the *weakest link fatigue damage* as

$$D_W(\boldsymbol{X}; N_y, N) := \frac{1}{W} \sum_{k=1}^{N_y} \frac{Z_k}{10^{\left(B_0 + B_1 \cdot G_{1,k}^* + B_2 \cdot G_{2,k}^*\right)}} \tag{9}$$

where

$$W := \min\left\{R_1, \ldots, R_N\right\} \tag{10}$$

denotes the deviation from median fatigue capacity for the weakest out of N chain links. The probability of failure for a segment of size N may then be expressed as

$$p_f^{(N)} = \mathrm{P}\left[D_{\text{cr}} \leq D_W(\boldsymbol{X}; N_y, N)\right] \tag{11}$$

which expresses the segment failure probability on the same format as that describing single link failure in Eq. (7). The derivation of Eq. (11) from Eqs. (7) and (8) is given in Appendix B.

3.2. Model uncertainties

We now introduce model uncertainties to account for inaccuracies in stress ranges, mean loads and corrosion grade.

[1] As an example: for a mooring chain segment composed of N identical links, each with the same failure probability, the ratio between the upper and lower bounds on the probability of segment failure (representing mutually independent or fully correlated failure events, respectively), is approximately proportional to N (see e.g., Melchers and Beck, 2018, Section 5.4).

[2] There are exceptions to this general rule, for instance in the presence of buoys. However, by definition, chain links on opposite sides of a buoy would be considered as parts of separate chain segments.

Stress ranges. Estimated stress ranges normally originate from one of the following sources: (i) mooring line tension measurements, (ii) mooring system response calculations or (iii) a combination of these. In the former case, measurement errors cause inaccuracies that will depend on for instance sensor type, time since last calibration and frequency resolution. In the case of response calculations, stress range errors arise from for instance inaccuracies in the numerical models (e.g., mooring component properties and environmental load coefficients for the floater), assumptions about operational parameters (e.g., draft and heading of floater, mooring line pretension) and the modeling of environmental loads (wind, waves and current). In general, the magnitude of the respective errors may be reduced by increasing the estimation effort, for instance by improved sensors or measurement techniques, by use of model tests for calibration of numerical models (Aksnes et al., 2015; Sauder, 2021) or by combining measurements and response calculations in a sensible way. The errors may, however, never be completely eliminated. For all cases, we assume that the *true* stress range may be quantified as $S' = Q_s \cdot S$, where Q_s is a random variable denoting stress range error and S is the estimated stress range. Assuming that Q_s is time-invariant and independent of the estimated stress range, the true fatigue load may then be expressed as

$$Z' = n_0 \int_S (Q_s \cdot s)^m f_S(s) ds = Q_s^m \cdot Z \tag{12}$$

where Z is the estimated fatigue load.

Mean loads. The mean load error is of similar nature and origin as that for the stress ranges, but is likely to be different in magnitude. For instance, if stress ranges and mean loads are taken from measurements, signal drift will directly influence the mean loads but not necessarily the dynamic loads (i.e., stress ranges) (Sauder et al., 2022). We therefore introduce a separate modeling error for the mean loads, and assume that the true mean stress may be expressed as $\sigma'_m = Q_m \cdot \sigma_m$, where Q_m is the mean load error and σ_m is the estimated mean stress. The true representative mean load is then obtained by substituting σ'_m for σ_m in Eq. (6)[3]:

$$G^{*}_{1,k}{}' = -\frac{1}{b_1} \log \left[\frac{\sum_i n_i \cdot s_i^m \cdot 10^{-b_1} \cdot g_1(Q_m \cdot \sigma_{m,i})}{n_{0,k} \cdot \mathrm{E}[S^m]_k} \right] \tag{13}$$

where $G^{*}_{1,k}{}'$ denotes the true representative mean load. This is inconvenient, since the numerator of the inner expression must be re-evaluated for each realization of the random variable Q_m. However, if the mean load function is on the form $g_1(\sigma_m) \propto \sigma_m$, the true representative mean load may be approximated as

$$G_1^{*\prime} \approx Q_m \cdot G_1^{*} \tag{14}$$

where G_1^* is the estimated representative mean load. An example demonstrating that the approximation error introduced by (14) is negligible for $g_1(\sigma_m) = \lambda_m$ is given in Appendix A.2.

Corrosion grade. A source of corrosion grade error is the categorization from inspections, in particular for the subjective scale used for the model described in Section 2. If a more objective scale were used, with categorization from for instance 3-D scans, the categorization error could be reduced but not fully eliminated.[4] Errors may also arise in the assumptions about the development of the corrosion grade between two inspection events. Analogously to the inclusion of stress range and mean load errors, we assume that the true corrosion grade may be expressed as $C' = Q_c \cdot C$ where Q_c is the corrosion grade categorization error and C is the estimated corrosion grade. The implications for the true representative value of the corrosion grade function, $G_2^{*\prime}$, then depends on the assumed form of the corrosion grade function, $g_2(c)$. For the function described in Section 2, $g_c(c) = c$, it is

$$G^{*}_{2,k}{}' = Q_c \cdot C_k \tag{15}$$

where C_k is the estimated corrosion grade for the kth year.

Fatigue damage including model uncertainty. An adjusted expression for the weakest link fatigue damage is now obtained by substituting true values $(Z', G_1^{*\prime}, G_2^{*\prime})$ for estimated values (Z, G_1^*, G_2^*) in Eq. (9):

$$D_W(\boldsymbol{X}; N_y, N) = \frac{1}{W} \sum_{k=1}^{N_y} \frac{Q_s^m \cdot Z_k}{10^{\left(B_0 + B_1 \cdot Q_m \cdot G^{*}_{1,k} + B_2 \cdot Q_c \cdot C_k\right)}} \tag{16}$$

where we have assumed that the approximation in (14) holds, and that the representation in (15) is applicable. Note that we have here implicitly assumed that the model uncertainties (Q_s, Q_m, Q_c) take on the same value for all components within a segment.

3.3. Limit state function

From the probability of segment failure in Eq. (11), we define the limit state function for fatigue failure of a chain segment as

$$g(\boldsymbol{X}; N_y, N) = D_{\mathrm{cr}} - D_W(\boldsymbol{X}; N_y, N) \tag{17}$$

where $D_W(\cdot)$ is the fatigue damage of the weakest link including model uncertainties, as defined in Eq. (16). The limit state function for single link failure is then obtained as a special case of (17), with $N = 1$ (in which case $W = R = 10^{\epsilon}$).

This concludes the reliability formulation for segment failure, including the effects of mean load and corrosion condition. In the next section we discuss some additional aspects of the reliability model.

4. Reliability formulation — additional aspects

In this section, we discuss the need for an extension of the formulation into considering failure of a mooring line, the distribution of the weakest link capacity, the difference between accumulated and annual failure probability and strategies to address the correlation between fatigue loads and mean loads.

4.1. Bounds on the failure of a mooring line

A mooring line is normally composed of more than one segment. The segments may be of the same type (e.g., all studless chains, possibly with different diameters), or they may be composed of different component types (e.g., chains and steel wire rope). In any case, it is a series system for which failure of any one segment leads to line failure. To formulate this, we first define the event E_j to denote fatigue failure for segment j, and $\bar{E}_j$ to denote its complement (the event that segment j survives):

$$\begin{aligned} E_j &: \quad g(\boldsymbol{X}_j; N_y, N_j) \le 0 \\ \bar{E}_j &: \quad g(\boldsymbol{X}_j; N_y, N_j) > 0 \end{aligned} \tag{18}$$

where N_j is the number of components in segment j. Note that to simplify the notation slightly, we have here assumed that the same limit state function, $g(\cdot)$, is applicable to all segments. In principle, however, it may differ for segments of different component types.

The probability of a mooring line fatigue failure may be expressed either by means of the event that any one segment fails, or by means of the complement of the event that all segments survive:

$$p_{f,\mathrm{line}} = \mathrm{P}\left[\bigcup_{j=1}^{J} E_j\right] = 1 - \mathrm{P}\left[\bigcap_{j=1}^{J} \bar{E}_j\right] \tag{19}$$

[3] Strictly, the true stress range S' should also be substituted for the estimated stress range S in Eq. (13). However, the stress range error (Q_s) cancels out since it enters the inner fraction in both numerator and denominator.

[4] See Gabrielsen et al. (2022) for preliminary results from ongoing work, aiming to develop computer algorithms that may be used to determine the corrosion grade based on 3-D scans of the chain links.

where J is the number of segments in the mooring line. To proceed from this point we would need to address the partial correlation of the segment failure events. A natural way forward could be to address the dependence or independence between the random variables contained in each random vector $\boldsymbol{X}_j$, similar to what was done for the partial dependence for the segment failure formulation. However, identical assumptions to those made for within-segment dependence and independence cannot necessarily be justified. Specifically;

- The S-N model coefficients will differ between segments with different component types.
- The fatigue loads will be highly correlated, but are likely to be of different magnitude due to for instance different component dimensions, damping effects along the line or even different stress range effect (S-N curve slope parameter, m, cf. Eqs. (1) and (4)).
- Mean loads are also highly correlated, but with magnitudes that depend on segment positions along the line.
- Corrosion grades may be anywhere between highly correlated (e.g., for segments that are close to each other and of similar component types) or completely uncorrelated (e.g., for segments in different positions along the line, such as fairlead chain vs. bottom chain, or for chain segments of different material grades).
- Replacement of individual segments, for any reason, leads to different number of years in service (N_y) between segments.

Hence, mooring line failure cannot be formulated in the same compact form as that for segment failure in the general case.

As an alternative to further developing Eq. (19), crude bounds may be given as (Melchers and Beck, 2018, Ch. 5):

$$\max_{j=1}^{J}\left\{\mathrm{P}[E_j]\right\} \le p_{f,\mathrm{line}} \le 1-\prod_{j=1}^{J}\left(1-\mathrm{P}\left[E_j\right]\right) \tag{20}$$

where the lower bound is exact for fully dependent failure events E_j whereas the upper bound is exact for completely independent events. Note that if the failure events are rare (i.e., $\mathrm{P}[E_j] \ll 1$ for all j), the upper bound may approximated by $p_{f,\mathrm{line}}^{(\mathrm{upper})} \approx \sum_{j=1}^{J}\mathrm{P}[E_j]$. For the general series system these bounds may be too wide to be of any practical value, but not necessarily for a mooring line with a limited number of segments.

As an example: (i) The narrowest bounds are obtained when the marginal failure probability for one of the segments is much larger than for the others. This critical segment will then define the lower bound, and also dominate the upper bound with minor contributions from the remaining segments. (ii) The widest bounds are obtained for the unlikely case that all segments are equally exposed to fatigue, with identical marginal failure probabilities. The upper bound will then be larger than the lower bound by a factor approximately equal to the number of segments, which is not particularly wide considering that structural reliability calculations are normally concerned with orders of magnitude rather than exact numbers.

In any case, the starting point for assessment of mooring line failure probability is to calculate the failure probability for each *segment* properly, and this is therefore the focus of the present paper. Note that an extension of a fatigue reliability formulation into considering failure of the critical segment in two adjacent mooring lines is presented and discussed by Mathisen and Hørte (2005).

4.2. Distribution of weakest link capacity

We will now elaborate on the distribution of W, defined in (10), describing the deviation from median fatigue capacity for the weakest link in a segment and used to define the weakest link fatigue damage in Eq. (9). Let ϵ be normally distributed with mean μ_ϵ and variance σ_ϵ^2, denoted $\epsilon \sim N(\mu_\epsilon, \sigma_\epsilon^2)$.[5] The random variable $R = 10^\epsilon$ then follows a lognormal distribution, denoted $R \sim LN(\mu_{\ln R}, \sigma_{\ln R})$ and defined by the cumulative distribution function (CDF)

$$F_R(r\,;\,\mu_{\ln R}, \sigma_{\ln R}) = \Phi\left(\frac{\ln r - \mu_{\ln R}}{\sigma_{\ln R}}\right) \tag{21}$$

where $\Phi(\cdot)$ is the standard normal CDF. The distribution parameters $\mu_{\ln R}$ and $\sigma_{\ln R}$ correspond to respectively mean value and standard deviation of the normal variate $\ln R$, and are thus given by

$$\mu_{\ln R} = \mathrm{E}[\ln R] = \ln 10\ \mu_\epsilon \tag{22}$$

$$\sigma_{\ln R} = \sqrt{\mathrm{Var}[\ln R]} = \ln 10\ \sigma_\epsilon \tag{23}$$

The exact distribution function for $W = \min\left\{R_1, \ldots, R_N\right\}$ is obtained from order statistics, see e.g., Bury (1999), as:

$$F_W(w; N) = 1 - \left[1 - F_R(w)\right]^N \tag{24}$$

Here, $F_R(\cdot)$ refers to the underlying (lognormal) single link distribution in (21), however; Eq. (24) is exact regardless of the underlying distribution type. Fig. 2 illustrates the effect of segment size on the distribution of W for the S-N model in Table 1, and shows that it is shifted towards lower capacity and becomes more narrow when the number of links increases.

Note that when the underlying distribution is lognormal, the distribution of the weakest link asymptotically (as $N \to \infty$) approaches the type III extreme value distribution of minima (Weibull) (Bury, 1999). Closed-form expressions for the Weibull distribution parameters based on those of the underlying lognormal distribution are given in Bury (1975). The Weibull distribution may be easier to work with, and is commonly available in software for probabilistic analysis. In general, however, using the exact distribution in (24) for numerical calculations is straightforward.

4.3. Accumulated vs. annual failure probability

The failure probability considered for the present work is on the form $p_f = \mathrm{P}[g(\boldsymbol{X}; t) \le 0]$, where t denotes time. In general, this quantity describes the point-in-time failure probability, and neglects the possibility that failure may have occurred at any point in time prior to t (i.e., that the event $g(\boldsymbol{X}; t') \le 0$ may have occurred for $t' < t$) (Straub et al., 2020). However; the limit state function for fatigue based on the S-N approach will decrease monotonically. The point-in-time probability expressed through the limit state function defined in (17), $p_f = \mathrm{P}[g(\boldsymbol{X}; N_y, N) \le 0]$, therefore represents an *accumulated* probability of failure for all years up to and including year N_y.

Design codes such as DNVGL-OS-E301 (DNV GL, 2018) are usually calibrated towards a target *annual* probability of failure. Following (Mathisen and Hørte, 2005), the annual failure probability may be expressed as the increase in accumulated probability from the year before, conditional on survival prior to the year considered. By introducing the notation $p_f(N_y) = \mathrm{P}[g(\boldsymbol{X}; N_y, N) \le 0]$ for the accumulated probability, this annual probability of failure is

$$p_{f,\mathrm{annual}} = \frac{p_f(N_y) - p_f(N_y - 1)}{1 - p_f(N_y - 1)} \tag{25}$$

Eq. (25) may be viewed as a discrete approximation to the hazard function (e.g., Straub et al., 2020) with year as the time unit, describing the annual failure rate conditional on survival up to and including N_y–1 years.

[5] Strictly, following the regression model in Eq. (3), we have $\mu_\epsilon := 0$. However, for the generality of the current subsection, we prefer to maintain the possibility for a non-zero μ_ϵ.

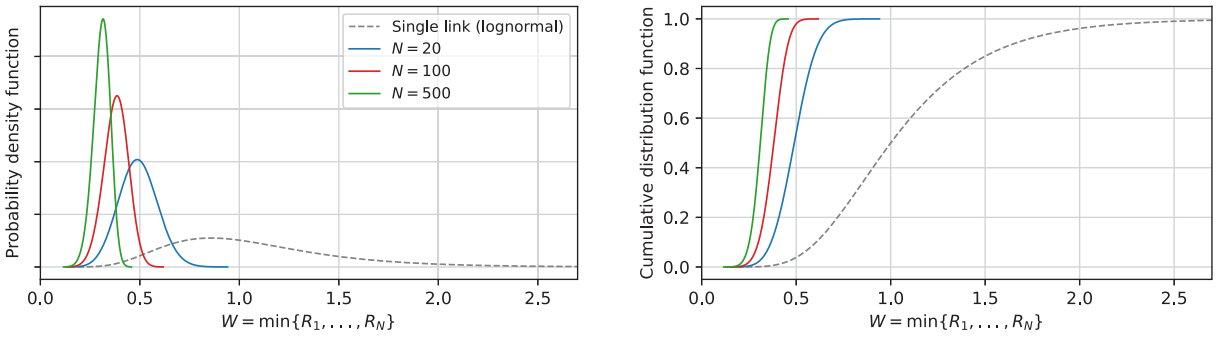

(a) Probability density function (PDF). (b) Cumulative distribution function (CDF).

Fig. 2. Example of distribution of W for $N \in \{20, 100, 500\}$, for $\epsilon \sim N(0, 0.17^2)$. Single link distribution included for comparison.

4.4. On the correlation between Z and G_1^*

The fatigue load (Z) and the representative mean load (G_1^*) originate from the same underlying load process, and may therefore be correlated with each other. Results presented in Lone et al. (2022, Sec. 3) for a typical production system in the Norwegian Sea showed that for each mooring line, the sign and magnitude of this correlation depend on its orientation compared to the dominating directions of environmental loads. Consequently, if the annual variability of Z and G_1^* is of importance for the problem at hand, the correlation between them may be important as well. In the following we will present three alternative ways to address this in the reliability calculations.

The first option it to model Z and G_1^* as dependent random variables. The practical implications of this approach will depend on the choice of method for dependence modeling and the calculation method for the reliability problem.

A second alternative is to introduce the random variable $Z^* = Z \cdot 10^{-B_1 \cdot G_1^*}$ as an "effective" fatigue load that includes the mean load effect on the capacity, as proposed in Lone et al. (2022). A probabilistic model for the variability of Z^* may then be established from joint statistics of Z and G_1^*, implicitly accounting for the correlation between them. Two premises are necessary for this approach to be useful. Firstly, the mean load coefficient (B_1) should be modeled as fixed. Otherwise, the probabilistic model for Z^* will depend on the random variable B_1, in which case the introduction of Z^* offers no convenience over modeling the correlation between Z and G_1^* as described in the first alternative. Secondly, inclusion of model uncertainties for stress ranges and mean loads to obtain the true value of the effective fatigue load yields $Z^{*\prime} = Q_s^m \cdot Z \cdot 10^{-B_1 \cdot Q_m \cdot G_1^*}$ (assuming that the approximation in Eq. (14) is applicable). This implies that the true effective fatigue load ($Z^{*\prime}$) cannot be expressed as an explicit function of the estimated effective fatigue load (Z^*) unless a fixed value is assumed for the mean load error (Q_m). A possible remedy could be to set a fixed value for the mean load error (typically, $Q_m = 1$), and substitute an alternative model uncertainty Q_{se} for Q_s to represent the total model error for the effective fatigue load. This new model uncertainty, Q_{se}, cannot be determined directly from Q_s and Q_m, and would then need to be estimated separately.

Finally, a third alternative is to neglect the dependence between Z and G_1^* and model them as mutually independent variable. This may be justified if (i) the correlation between them is weak, or (ii) the annual variability of Z and G_1^* is shown to be of limited importance for the quantity of interest, or (iii) the correlation between Z and G_1^* is found to be negative (if the correlation between them is negative, implying that a high fatigue load is likely to be combined with a low mean load, the assumption of independence will be conservative with respect to fatigue damage). This third approach, assuming independence, will be applied in the case study in Section 5.

5. Case study

As a case study, we consider fatigue of a mooring chain segment, and the case study is divided into three parts: (i) A *global sensitivity analysis*, to identify random variables that may be fixed in order to simplify the fatigue damage model and reduce the dimension of the problem, and assess the importance of interactions between random variables in the model. (ii) A *reliability analysis*, to calculate the probability of fatigue failure for the base case, validate the selected approach, and assess the importance of the respective variables. (iii) Additional findings, from parameter variation and comparison to alternative S-N models neglecting mean load or corrosion effects.

5.1. Basis

The base case is partly related to the case study presented in Lone et al. (2022), but with higher fatigue loads. We consider a service life of 15 years for a segment with 500 chain links. Fatigue capacity is described by a S-N model with stress range effect $m = 3$, and intercept parameter according to Eq. (2) with $g_1(\sigma_m) = \lambda_m$ [% MBL] and $g_2(c) = c$. Probability distributions applied for the random variables in the base case are listed in Table 2, and are defined on the basis described in the subsequent paragraphs.

Critical damage. Wirsching and Chen (1988) list statistics for the uncertainty in Miner's sum at failure from various sources, with median values ranging from 0.69 to 1.15 and coefficient of variation (CoV) ranging from 0.19 to 0.67. In their example of tendon fatigue for a tension-leg platform they modeled it as a lognormal variable with a median value of 1.0 and a CoV of 0.30. This model has since been widely used for fatigue reliability of marine structures, including the DNVGL-OS-E301 design code calibration (Mathisen and Hørte, 2005) and the JCSS probabilistic code for fatigue (JCSS, 2011), and is also used for D_{cr} in the present study.[6]

Weakest link resistance. The weakest link resistance, W, is defined indirectly by means of the S-N model regression error, ϵ, representing deviation from the median fatigue capacity of individual links. The model corresponds to the S-N model defined in Table 1. For the calculations in the present study, the exact distribution of W as defined in Eq. (24) is used.

[6] Strictly, JCSS (2011) suggests that the Miner's sum uncertainty is modeled as lognormal with *mean* 1.0, whereas Wirsching and Chen (1988) suggested a *median* value of 1.0. The latter is adopted here, and corresponds to a mean value of 1.04 with a CoV of 0.30.

Table 2
Random variables for base case. The basis for the probability distributions applied is described in the main text.

Variable	Symbol	Unit	Dimension[a]	Distributed as	Mean	St.dev.	CoV[b]
Miner's sum at failure	D_{cr}	–	1	$LN(0, 0.29)$	1.04	0.31	0.30
Predictive uncertainty of S-N model	ϵ	–	1	$N(0, 0.17^2)$	0	0.17	–
Time-invariant term of S-N intercept	B_0	–	1	see note[c]	12.249	0.088	–
Mean load effect	B_1	–	1	see note[c]	−0.0507	0.0045	–
Corrosion grade effect	B_2	–	1	see note[c]	−0.106	0.0075	–
Annual fatigue loads	Z	MPa^3	N_y	$LN(19.96, 0.39)$	5×10^8	2×10^8	0.40
Annual representative mean loads	G_1^*	% MBL	N_y	$N(15.0, 0.6^2)$	15.0	0.6	0.04
Corrosion grade at end of service life	C_{end}	–	1	$U(1, 7)$	4	1.7	–
Model uncertainty (stress ranges)	Q_s	–	1	$N(1.0, 0.10^2)$	1.0	0.10	0.10
Model uncertainty (mean loads)	Q_m	–	1	$N(1.0, 0.10^2)$	1.0	0.10	0.10
Model uncertainty (corrosion grade)	Q_c	–	–	Fixed	1.0	–	–

Dimension: number of random variables. St.dev.: standard deviation. CoV: coefficient of variation.
[a]Number of i.i.d. random variables with this distribution.
[b]CoV is given when used to define the distribution.
[c]Multivariate normal with covariance matrix given in Eq. (26). Listed standard deviations correspond to the square roots of the diagonal terms of the covariance matrix.

S-N model intercept coefficients. The uncertainty in the coefficients of the S-N model intercept parameter, $(B_j)_{j\in\{0,1,2\}}$, represents the inferential uncertainty (see e.g., Gelman and Hill, 2007) of the regression model in Eq. (3). They are jointly distributed according to a multivariate normal distribution, $N(\boldsymbol{\mu}, \boldsymbol{\Sigma})$, with mean vector $\boldsymbol{\mu}$ defined from the least-squares estimates in Table 1 and covariance matrix (Lone et al., 2022)

$$\boldsymbol{\Sigma} = \begin{bmatrix} 7.770\times10^{-3} & -3.829\times10^{-4} & -4.453\times10^{-4} \\ -3.829\times10^{-4} & 2.046\times10^{-5} & 1.714\times10^{-5} \\ -4.453\times10^{-4} & 1.714\times10^{-5} & 5.612\times10^{-5} \end{bmatrix} \tag{26}$$

In Lone et al. (2022), the inferential uncertainty of the B_j coefficients was found to be non-influential for the fatigue damage of the lines considered. This is reassessed in the present study, including the importance of possible interactions with other random variables.

Fatigue loads. The probability distribution assigned to Z represents the annual variability of the fatigue loads. Hence, N_y i.i.d. random variables are needed to model the fatigue damage after N_y years. The expected value is increased compared to those reported for the mooring system considered in Lone et al. (2022), and is here set to $E[Z] = 5\times10^8$. This is the maximum annual fatigue load that meets the design code requirements in DNVGL-OS-E301 (DNV GL, 2018) with a fatigue safety factor of 8 without accounting for corrosion in any way.[7] The underlying calculations to obtain this value are given in Appendix C. For the mooring lines considered in Lone et al. (2022), the CoV of Z was found to be in the range 0.24–0.38. In the base case of the present study we set the CoV to 0.40, just above the upper value of the given range. The annual fatigue loads are assumed to follow a lognormal distribution, based on the test-of-fit results reported in Lone et al. (2022).

Representative mean loads. As for the fatigue loads, the probability distribution assigned to G_1^* represents the annual variability of the representative mean load. For the present study we assume an expected value of 15 [% MBL] and a CoV of 0.04. The mean value is slightly higher than that reported for the mooring lines considered in Lone et al. (2022). However, the mean load is sensitive to parameters such as chain dimension and material grade, operational measures (e.g., pretension), type of unit and orientation of line, so any value from 10% to 20% MBL (or even outside this range in certain cases) is of relevance for the study. The selected CoV is in the high end of the range reported in Lone et al. (2022) (0.02–0.04). For convenience, the annual mean loads are assumed to follow a normal distribution. Furthermore, they are assumed to be independent of the annual fatigue loads, which implies that the possible correlation between them is neglected. This latter choice will be assessed in connection with the global sensitivity analysis.

Corrosion grade. We assume that nothing is known about the corrosion grade of the segment, either because the assessment is performed prior to operation or because inspections have not been carried out. The only information available is then that the grade is bounded by its value at installation ($c = 1$) and what is presently considered as the upper limit of the corrosion grade scale ($c = 7$). One could imagine that more narrow bounds for the most likely corrosion grade development could be defined based on previous experience for similar chain segments (e.g., comparable depth and location along line), but this is not addressed here. Hence, the corrosion grade at the end of the service life, C_{end}, is modeled as a uniform variable with support $[1, 7]$, in accordance with the maximum entropy principle (Kapur, 1989). A deterministic temporal development is assumed, with the corrosion grade evolving linearly from $c = 1$ in the first year to its value at end of service life.

Model uncertainties. We here apply normal distributions with a mean of 1.0 and a CoV of 0.10 to model the uncertainty in both stress ranges and mean loads (Q_s and Q_m, respectively). As accurate quantification of the model uncertainties is beyond the scope of the present study, these should be interpreted as notional values. For corrosion grade, the model uncertainty is here fixed to 1.0. The rationale is that in the present study, we have already modeled complete ignorance about the value of the corrosion grade, C_{end}.

Model dimension and dependence between variables. In summary, the base case probabilistic model has a dimension of $8 + 2 \cdot N_y$, that is, 38 random variables are used to evaluate the limit state function at the end of the service life of 15 years. These random variables are all assumed to be mutually independent, except for the B_j coefficients of the S-N model which are jointly distributed according to a multivariate normal distribution.

5.2. Method

The primary objective of the global sensitivity analysis for the present study is to identify variables that may be fixed in order to reduce the model dimension. A secondary objective is to assess the amount of non-additive interactions in the model. These are achieved by employing a set of variance-based sensitivity measures known as the Sobol' indices (Sobol', 1993). A brief description of the Sobol' indices is given in Appendix D. For the present study, they are estimated by Monte Carlo simulation (MCS), applying the sampling scheme and estimators proposed by Saltelli et al. (2010) with sample size 10^6. Interdependent variables (B_0, B_1, B_2) are grouped to satisfy the requirement

[7] The relation between the expected annual fatigue load and the design code requirements is given for convenience, and should not be interpreted as an attempt to quantify the safety level inherent in DNVGL-OS-E301 (DNV GL, 2018).

of independent variables (Jacques et al., 2006). In addition, the annual representative mean loads ($G^*_{1,k}$) and the annual fatigue loads (Z_k) are grouped, respectively. The associated Sobol' indices then quantify the effect of each group of components combined.

The objective of the reliability analysis is to calculate the probability of failure, p_f, by computing

$$p_f = \mathrm{P}[g(\boldsymbol{X}) \le 0] = \int_{g(\boldsymbol{X})\le 0} f_{\boldsymbol{X}}(\boldsymbol{x})\, d\boldsymbol{x} \tag{27}$$

where $g(\boldsymbol{X})$ is the limit state function given in Eq. (17) and $f_{\boldsymbol{X}}(\cdot)$ is the joint PDF of the random vector $\boldsymbol{X}$. For the present study, we first approximate (27) by the first-order reliability method (FORM). The FORM result is then used as the basis for estimating the integral more accurately by importance sampling. FORM-based sensitivity measures applied in the case study – the FORM importance factors and the omission sensitivity factors – are described in Appendix D.

The FORM analysis is performed by identifying the design point, $\boldsymbol{u}^*$, satisfying

$$\boldsymbol{u}^* = \arg\min \left\{ \|\boldsymbol{u}\| \,;\; g_{\boldsymbol{U}}(\boldsymbol{u}) \le 0 \right\} \tag{28}$$

where $\boldsymbol{U} \in \mathbb{R}^M$ represents an isoprobabilistic transformation of the vector $\boldsymbol{X}$ in physical space to an independent vector in standard normal space, $\boldsymbol{U} = T(\boldsymbol{X})$; and $g_{\boldsymbol{U}}(\boldsymbol{u}) = g(T^{-1}(\boldsymbol{u}))$ is the limit state function evaluated for a point in the transformed U-space. The FORM probability of failure is obtained from

$$p_{f,\mathrm{FORM}} = \Phi(-\beta) \tag{29}$$

where $\beta = \|\boldsymbol{u}^*\|$ is the FORM reliability index, defined as the distance from the origin of the U-space to the design point. FORM is exact only if the limit state surface is linear in U-space, and the accuracy of the approximation depends on its shape at the design point and the dimension of the problem (Lemaire, 2009, pp. 173 and 214).

The importance sampling estimate of the failure probability, $\hat{p}_{f,\mathrm{IS}}$, is obtained from MCS with independent standard normal sampling distributions centered at the FORM design point in the transformed U-space. This ensures efficient low-variance estimates of the failure probability (Melchers and Beck, 2018). A sample size of 10^4 is used in the present study. For further details on FORM and importance sampling, see e.g., Lemaire (2009), Melchers and Beck (2018).

5.3. Results and discussion

5.3.1. Global sensitivity analysis

Sobol' indices for weakest link fatigue damage in the final year of the base case are presented in Fig. 3. Firstly – and most importantly – the total effect indices are close to zero for B_j and for G_1. This means that the inferential uncertainty of the S-N curve coefficients and the annual variability of the representative mean loads are practically non-influential. Further implications are that (i) the simplification introduced by neglecting possible correlation between annual fatigue loads (Z) and mean loads (G^*_1) is justified, and (ii) (B_0, B_1, B_2) and G^*_1 may be fixed to their respective mean values for the subsequent reliability analysis with negligible impact on the estimated failure probability. Secondly, the sum of the first-order indices is $\sum_i S_i = 0.927$, meaning that roughly 7% of the fatigue damage uncertainty is caused by non-additive interaction effects. Judging by the difference between S_{Ti} and S_i, the variables with the most interaction are Q_s and C_{end} (although, not necessarily just with each other), followed by Q_m and W. Thirdly, the importance of modeling the annual variability of the fatigue loads (Z) is seen to be limited but not negligible, contributing to around 6% of the fatigue damage uncertainty in total.

The influence of the annual fatigue loads is investigated in more detail by assessing sensitivity indices for the fatigue load during each year, shown in Fig. 4. Both the first-order and the total effect indices for Z_k increase with increasing k, meaning that the fatigue loads experienced during the last years influence the fatigue damage uncertainty more

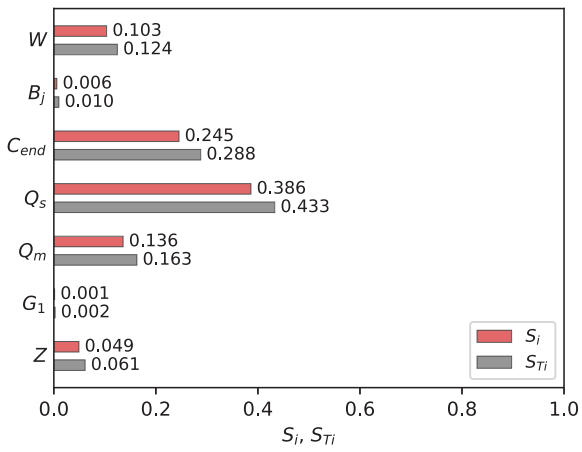

Fig. 3. Sobol' indices for weakest link fatigue damage in final year of base case: $D_W(\boldsymbol{X}; N_y = 15, N = 500)$. See Table 2 for a description of the variables. S_i = first-order index; S_{Ti} = total-effect index.

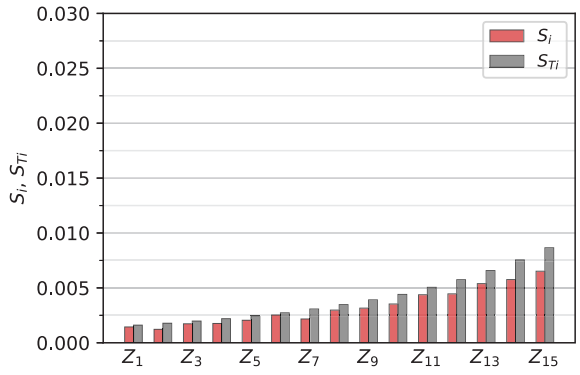

Fig. 4. Sobol' indices for effect on $D_W(\boldsymbol{X}; N_y = 15, N = 500)$ from annual fatigue load uncertainty. Note the scale of the vertical axis. S_i = first-order index; S_{Ti} = total-effect index.

than those experienced during early years. The reason is the following. The expected corrosion grade increases with time, causing a temporal degradation of the median fatigue capacity. Uncertainty in annual fatigue load for the last years will therefore yield larger contributions to fatigue damage variance than uncertainty in fatigue loads for the first years. This effect causes the increase in the first-order index, S_i. The relatively larger increase in the total-effect index (S_{Ti}) is because the corrosion grade uncertainty also increases with time, interacting with the fatigue load uncertainty in the final years. Nevertheless, the total-effect index of the annual fatigue loads combined (Fig. 3) suggests that these interactions are of limited importance.

5.3.2. Reliability analysis for base case

Based on the global sensitivity analysis, the S-N curve coefficients (B_0, B_1, B_2) and the annual mean loads G^*_1 are now fixed to their expected values. This reduces the dimension of the model to $M = 5 + N_y$, that is, $M = 20$ random variables to calculate the failure probability after $N_y = 15$ years. Furthermore, the remaining random variables may be assumed to be mutually independent.

Failure probabilities for the final year of the base case are shown in Table 3. Accumulated and annual failure probabilities differ by a factor of around 1.7, with the annual failure probability on the low side. The temporal development of both quantities is compared in Fig. 5, showing that the difference occurs mainly towards the end of the service life as the accumulated failure probability increases less steeply. In any case, the limited ratio between these quantities suggests that the use of either one over the other is unlikely to be decisive for the problem at hand.

Table 3
Results for the failure probabilities. Base case, final year ($N_y = 15$).

	Accumulated	Annual
β	3.63	
$p_{f,\mathrm{FORM}}$	1.42×10^{-4}	8.55×10^{-5}
$\hat{p}_{f,\mathrm{IS}}$	1.86×10^{-4}	1.08×10^{-4}
$\mathrm{CoV}(\hat{p}_{f,\mathrm{IS}})$	0.02	

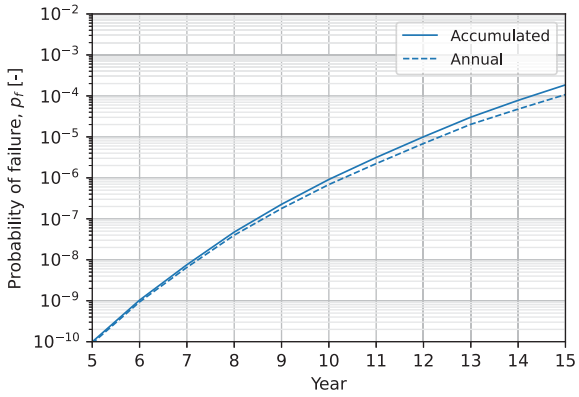

Fig. 5. Probability of failure for the last 10 years of the base case: accumulated vs. annual failure probabilities.

FORM importance factors are visualized in Fig. 6. The most influential variables are the critical fatigue damage (D_{cr}) and the stress range uncertainty (Q_s). The somewhat limited importance of W is due to the segment size of $N = 500$, resulting in a fairly narrow distribution for the weakest link capacity (cf. Fig. 2). A smaller segment size would yield a wider distribution and increase the relative importance of W.

A limited importance factor is observed also for the corrosion grade uncertainty (C_{end}). This may be explained by considering a 2-dimensional section through the design point and the failure surface ($g_{\boldsymbol{U}}(\boldsymbol{u}) = 0$) in standard normal space, shown in Fig. 7. The distance from the failure surface to the origin of the U-space increases rapidly with increasing value for $U_3 = T_3(C_{\mathrm{end}})$, meaning that no substantial contribution to the failure probability is obtained from going further into the tail of the distribution of C_{end}. This effect is a consequence of the corrosion grade scale applied. For the present work it is defined with an absolute upper limit of $c = 7$, as reflected by the uniform distribution used to model its uncertainty. Any degradation of the chain larger than that prescribed by $c = 7$ is thus precluded. Hence, it might be in its place to consider the need for a probability distribution that allows the corrosion grade to exceed 7, however small the probability.

Lastly, the importance of annual fatigue load variability is low, with the sum of the importance factors for Z_k at only 4.3%. The corresponding omission sensitivity factor is 1.02 if the fatigue load in each year is fixed to its expected value. For the reliability index given in Table 3, this implies that the (FORM) failure probability is underestimated by a factor of $\Phi(-\beta)/\Phi(-\beta \cdot 1.02) \approx 1.3$ if the annual fatigue load variability is neglected, an error that may be considered negligible in this context. Hence, despite some interaction with the corrosion grade uncertainty, Z may be fixed to its expected value with minor impact on the failure probability in the final year for the present case.

5.4. Additional findings

5.4.1. Effect of fatigue load and representative mean load

The effect on probability of fatigue failure from expected annual fatigue load and representative mean load is now assessed. Results for the last ten years of the service life are presented in Fig. 8, in terms of annual failure probability obtained from importance sampling.

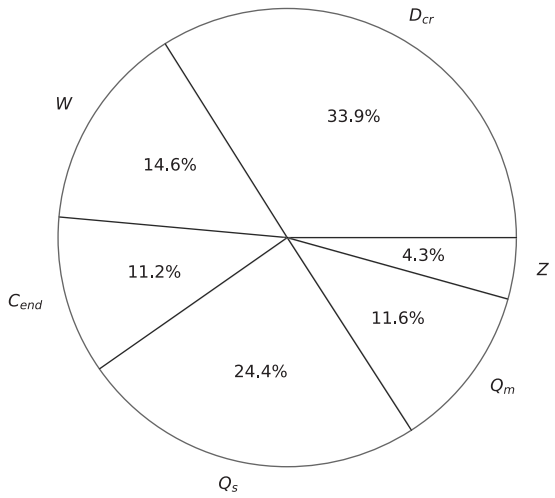

Fig. 6. FORM importance factors, α_i^2. Importance factor for Z is the sum of α_i^2 for $(Z_k)_{k\in\{1,\ldots,N_y\}}$.

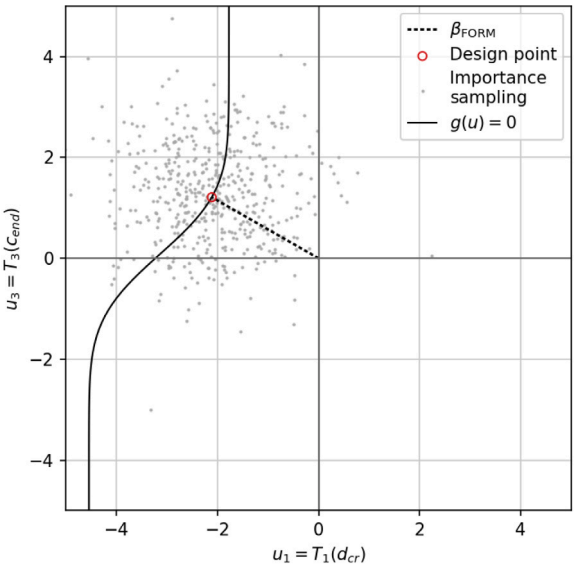

Fig. 7. FORM design point in standard normal space for C_{end} and D_{cr}, along with a section of the failure surface and 500 points from the importance sampling.

Expected annual fatigue load. In Fig. 8(a), the expected annual fatigue load is varied by ±20% and ± 40% compared to the base case value. With stress range effect $m = 3$, this corresponds to adjustments of the nominal chain diameter ranging from −5% to +10% (for highest and lowest fatigue loads, respectively) – if one assumes that the tension range distribution is unaffected by the change in diameter.[8] The expected fatigue damage is directly proportional the to mean annual fatigue load (cf. Eq. (16)), and thus increases by the same factor as $\mathrm{E}[Z]$. This has a substantial effect on the failure probability. An increase of $\mathrm{E}[Z]$ by 40% increases the probability of failure by one order of magnitude in the final year, whereas a reduction of $\mathrm{E}[Z]$ by 40% reduces it by nearly two orders of magnitude.

Representative mean load. The effect of the representative mean load is shown in Fig. 8(b), for mean loads ranging from 10% to 20%

[8] In practice, a change in chain diameter will also affect the mean load measured in percentage of MBL, and thereby affect the failure probability also through a reduction or increase in fatigue capacity.

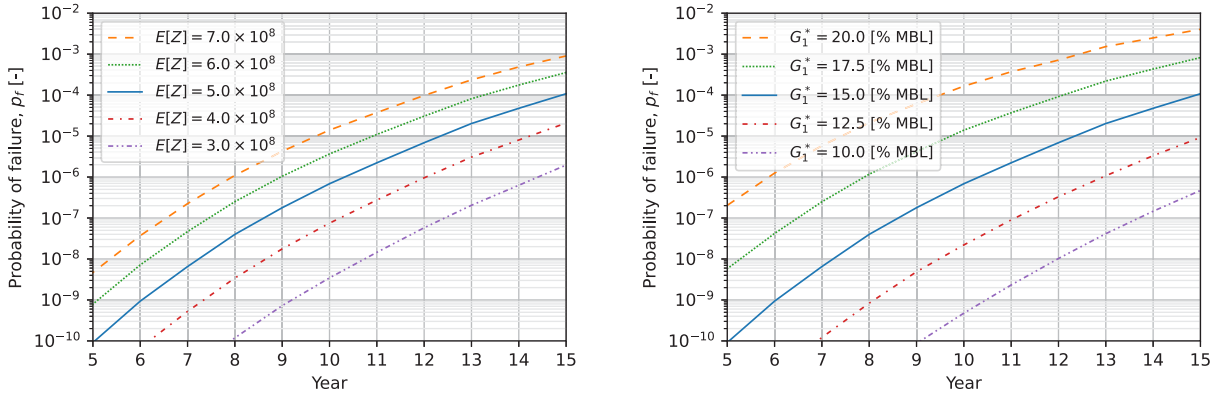

(a) Expected annual fatigue load.

(b) Representative mean load.

Fig. 8. Effect of fatigue load and representative mean load on probability of failure. Base case result is shown by solid blue line in both subfigures.

of MBL — all of which are realistic mean load levels for offshore mooring systems. The mean load effect on the fatigue capacity is seen to significantly impact the fatigue reliability. Compared to the base case at 15% MBL, a change in mean load by ±2.5% MBL increases or reduces the failure probability by approximately one order of magnitude. This is a slightly larger effect than that obtained for a change in $E[Z]$ by ±20% (Fig. 8(a)). For mean load 10% MBL the failure probability is more than two orders of magnitude below the base case, whereas for 20% MBL it is higher by a factor of 40.

5.4.2. Effect of segment size

In Fig. 9, the segment size is varied between $N = 1$ (single link) and $N = 500$. In terms of probability of failure in the last year, a reduction of segment size from $N = 500$ to $N = 20$ is comparable to a reduction of the expected annual fatigue load by a little more than 20% (Fig. 8(a)) or a reduction of the representative mean load by 2.5% MBL (Fig. 8(b)).

These results may also be used as a basis to assess the effect of the assumptions related to dependence and independence between links. If we consider a simplified treatment of dependence between links, the upper bound of the segment failure is $p_f^{(N)} \leq 1 - (1 - p_f^{(1)})^N$ (corresponding to independent failure events for each of the links). From Fig. 9 we obtain $p_f^{(1)} = 4 \times 10^{-7}$, which gives the upper bound $p_f^{(500)} \leq 2 \times 10^{-4}$. Compared to the value obtained here, $p_f^{(500)} \approx 1 \times 10^{-4}$, the upper bound is larger only by a factor of 2 (which is quite modest in connection with failure probabilities, for which orders of magnitude are most important). This means that the current reliability formulation yields results that correspond closely to independent failure events. In other words, the assumption that ϵ_i is independent between links has, in practice, a much stronger effect on the failure probability than the assumption of variables that are fully dependent between links (i.e., $D_{\text{cr}}, Z, C_{\text{end}}, Q_s$ and Q_m among those that have not been fixed).

5.4.3. Treatment of mean load and corrosion effects

Alternative ways of treating mean load and corrosion effects are now addressed. Referring to the legend of Fig. 10, the cases considered are defined as follows:

(1) *Excl. mean load effect*. Mean load effect on fatigue capacity is neglected, i.e., fixed values $G_1^* = 20$ [% MBL] and $Q_m = 1$ are used.
(2) *Excl. corrosion effect*. Degradation due to corrosion is neglected, by fixing $C_{\text{end}} = 1$.
(3) *Excl. mean load and corrosion effects*. The first two cases combined.
(4) *Excl. mean load, incl. corr. rate*. Same as the previous case, but corrosion is accounted for by a reduction of the cross section area, expressed though a corrosion rate describing the annual material loss. See Appendix C for related calculations. We have assumed that the nominal diameter is 120 mm, and a (fixed) corrosion rate of 0.4 mm/year is applied.

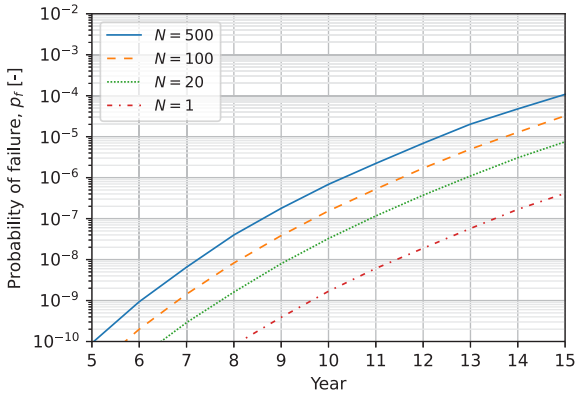

Fig. 9. Effect of segment size (N links) on probability of failure.

Note that the last case resembles how corrosion is accounted for in the current design code approach (DNV GL, 2018).

The results in Fig. 10 show that the failure probability is significantly overestimated if one neglects the mean load effect while at the same time accounting for degradation due to corrosion (case 1). Conversely, the failure probability is underestimated by even more if the beneficial effect of a mean load below 20% is realized without accounting for corrosion (case 2). When both mean load and degradation are neglected (case 3), the failure probability increases less steeply with time. Compared to the base case, it is overestimated for the early years and underestimated for the final years. A similar development of the failure probability with time is seen for the case with a simplified corrosion model (case 4), slightly on the high side of the previous case. Coincidentally, the failure probability in the final year matches that obtained for the base case. However; (i) the apparent agreement would not be seen if a different mean load had been applied for the base case, and (ii) the failure probability in subsequent years would most likely be underestimated by the simplified approach, considering the different slopes of the curves.

6. Conclusions

A reliability formulation for fatigue failure of mooring chain segments that accounts for the effects on fatigue capacity from mean load and degradation due to corrosion has been presented. The limit

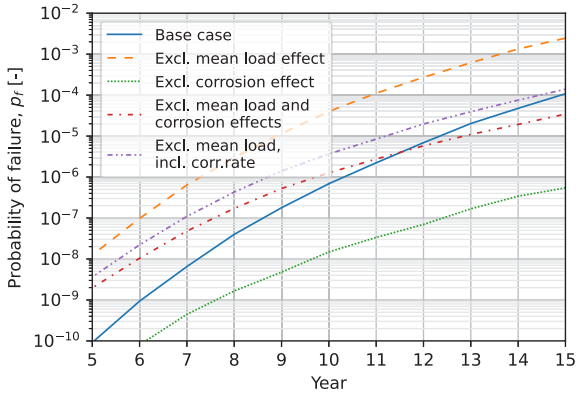

Fig. 10. Effect on probability of failure from alternative treatments of mean load and corrosion effects.

state function is defined from a summation of the fatigue damage contribution per year of service, which enables accounting for (i) both known fatigue loads during prior years of service and future, uncertain loads, and (ii) the temporal development of the corrosion condition of the chain.

Partial dependence between the failure events of individual links within a segment is handled by distinguishing between variables that are either independent between links or fully dependent and take on the same values. This leads to a weakest link formulation, making it straightforward to assess the fatigue reliability for arbitrary segment size.

As part of the case study, a global sensitivity analysis was used to identify non-influential variables and to assess the amount of interactions in the model. For the applied S-N model and the case defined for the present study it was found that (i) the S-N curve coefficients (B_0, B_1, B_2) and the annual representative mean load (G_1^*) may be fixed to their mean values with negligible impact on the fatigue damage variance, and (ii) the random variables interact moderately within the model, with interactions contributing around 7% of the uncertainty in fatigue damage after 15 years for the base case.

A reliability analysis was conducted thereafter, including variation of model parameters. The main findings were the following:

- The relative importance of uncertainty in corrosion grade is constrained by the choice of a uniform distribution to represent it, thereby restricting the maximum degradation of the chain.
- Annual fatigue load variability has insignificant influence on the failure probability in the final year, despite temporal degradation of the fatigue capacity and some degree of interaction with the corrosion grade uncertainty.
- The formulation for *segment* failure gives results that are close to those obtained if independent events with identical probabilities are assumed for failure of individual links. This indicates that the assumption of independent S-N model regression errors has a stronger effect on the reliability than the assumptions that all the links are exposed to the same loads and degradation, and that they fail at the same critical level of fatigue damage.
- Mean load and degradation due to corrosion both have a substantial impact on the failure probability. These effects have, in practice, opposite consequences for fatigue life. *Coincidentally*, for the particular case considered here, including both effects leads to similar failure probability at end of service life as neglecting both. This is not true in general.
- Accounting for corrosion in a simplified way, through a corrosion rate describing the annual reduction of the chain diameter (and a corresponding increase in fatigue load), considerably underestimates the corrosion effect on fatigue reliability compared to that predicted by the S-N model used for the present study.

The case study results support the need for a fatigue reliability formulation that accounts properly for mean load and chain degradation.

CRediT authorship contribution statement

Erling N. Lone: Conceptualization, Methodology, Software, Formal analysis, Data curation, Visualization, Writing – original draft, Editing. **Thomas Sauder:** Conceptualization, Writing – review & editing, Supervision. **Kjell Larsen:** Conceptualization, Writing – review & editing, Supervision. **Bernt J. Leira:** Conceptualization, Writing – review & editing, Supervision, Funding acquisition.

Declaration of competing interest

The authors declare that they have no known competing financial interests or personal relationships that could have appeared to influence the work reported in this paper.

Data availability

The authors do not have permission to share data.

Acknowledgment

This study was financed by the Research Council of Norway, through the project 280705 “Improved lifetime estimation of mooring chains” (LIFEMOOR).

Appendix A. Examples

A.1. Representative mean load: insensitive to variations in mean load coefficient

We consider the hindcast-based simulations presented in Lone et al. (2022) for the mooring system of a typical semi-submersible production unit in the Norwegian Sea. The current calculations are performed for mooring line 1 of the system considered, see Lone et al. (2022, Sec. 3) for details. Representative mean load is calculated for the years 2001–2010 using Eq. (6) with the mean load function $g_1(\sigma_m) = \lambda_m$ [% MBL] and three different values of b_1: the estimated value from regression analysis, $\hat{B}_1 = -0.0507$ (Table 1), and $\hat{B}_1 \pm 2 \cdot \hat{\sigma}_{B_1}$ where $\hat{\sigma}_{B_1} = 0.0045$ is the estimated standard error of $\hat{B}_1$ (Lone et al., 2022, Sec. 4). The resulting values for g_1^* are presented in Fig. A.11, showing negligible difference for the lower and upper values of the estimated representative mean load for each year. Hence, for the S-N model in Table 1 and the mooring line considered in the current example, a fixed value of B_1 may be used for the calculation of representative mean load, regardless of whether a fixed or stochastic mean load coefficient is assumed for the probabilistic analysis.

A.2. Approximation to true representative mean load

A comparison of the true representative mean load calculated by means of Eqs. (13) (“exact”) and (14) (“approximation”) is shown in Fig. A.12 for two realizations q_m of the mean load error with $g_1(\sigma_m) = \lambda_m$ [% MBL].

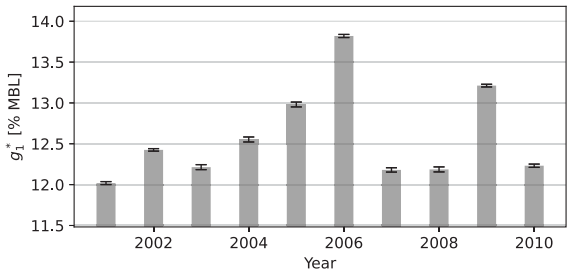

Fig. A.11. Example of annual representative mean loads for a semi-submersible in the Norwegian Sea, calculated for $b_1 = \hat{B}_1$ (bars) and $b_1 = \hat{B}_1 \pm 2 \cdot \hat{\sigma}_{B_1}$ (error bars). The limits of the vertical axis have been narrowed down to make the upper and lower values of the error bars distinguishable.

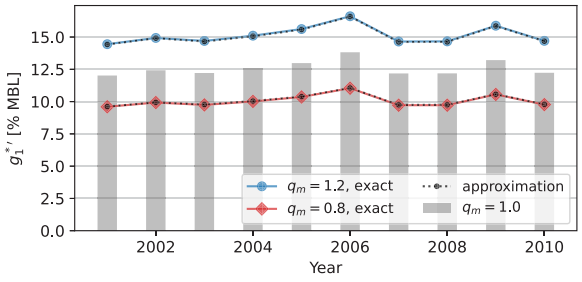

Fig. A.12. Comparison of true representative mean loads evaluated by Eqs. (13) ("exact") and (14) ("approximation") for $q_m \in \{0.8, 1.2\}$ with $g_1(\sigma_m) = \lambda_m$ [% MBL], using the same joint stress range and mean load distribution as applied for Fig. A.11. Representative mean loads for $q_m = 1.0$ are included for reference.

Appendix B. Weakest link-based segment failure formulation

Derivation of the segment failure probability in Eq. (11) from the single link failure probability in Eq. (7) and the fatigue damage of the ith component in Eq. (8).

The failure probability of the ith component is

$$p_f^{(i)} = \mathrm{P}\left[D_{\mathrm{cr}} \leq \frac{1}{R_i} \sum_{k=1}^{N_y} \frac{Z_k}{10^{\left(B_0 + B_1 \cdot G_{1,k}^* + B_2 \cdot G_{2,k}^*\right)}} \right] \tag{B.1}$$

By defining the auxiliary variable

$$V(\boldsymbol{X}; N_y) := \frac{1}{D_{\mathrm{cr}}} \sum_{k=1}^{N_y} \frac{Z_k}{10^{\left(B_0 + B_1 \cdot G_{1,k}^* + B_2 \cdot G_{2,k}^*\right)}} \tag{B.2}$$

and utilizing that R and D_{cr} are always positive, Eq. (B.1) may be reorganized into

$$p_f^{(i)} = \mathrm{P}\left[R_i \leq V(\boldsymbol{X}; N_y) \right] \tag{B.3}$$

The probability of segment failure may now be expressed by means of the event that any of the N links fails or, equivalently, as the complement of the event that all the components survive:

$$p_f^{(N)} = \mathrm{P}\left[\bigcup_{i=1}^{N} (R_i \leq V(\boldsymbol{X}; N_y)) \right] = 1 - \mathrm{P}\left[\bigcap_{i=1}^{N} (R_i > V(\boldsymbol{X}; N_y)) \right] \tag{B.4}$$

By conditioning on a realization of the variables that are fully correlated between links, $v = V(\boldsymbol{x})$, the failure (or survival) events become statistically independent. Recalling that the R_i are i.i.d., the conditional probability of segment failure is then

$$p_{f|\boldsymbol{X}=\boldsymbol{x}}^{(N)} = 1 - \prod_{i=1}^{N} \mathrm{P}\left[R_i > v\right] \; = 1 - \mathrm{P}\left[R > v\right]^N \; = 1 - \left[1 - F_R(v)\right]^N \tag{B.5}$$

where $F_R(v) = \mathrm{P}[R \leq v]$ is the CDF of R for any single link, evaluated at v. From order statistics, the resulting expression is recognized as the exact distribution of the extreme minimum value of N i.i.d. variables R, see e.g., Bury (1999). The conditional probability in (B.5) may thus be expressed in a more compact form as $p_{f|\boldsymbol{X}=\boldsymbol{x}}^{(N)} = F_W(v; N)$, where $F_W(\cdot)$ denotes the CDF of $W = \min\{R_1, \ldots, R_N\}$. The marginal segment failure probability is then obtained from the total probability theorem as

$$p_f^{(N)} = \int_{\boldsymbol{X}} F_W(V(\boldsymbol{x}); N) \; f_{\boldsymbol{X}}(\boldsymbol{x}) \, \mathrm{d}\boldsymbol{x} \tag{B.6}$$

where $f_{\boldsymbol{X}}(\cdot)$ is the joint probability density function for $\boldsymbol{X}$. This resulting integral is equivalent to the probability statement (see e.g., Lemaire, 2009, Ch. 3)

$$p_f^{(N)} = \mathrm{P}\left[W \leq V\right] \tag{B.7}$$

Finally, by introducing the weakest link fatigue damage defined in (9), Eq. (B.7) may be reorganized into the segment failure probability in Eq. (11).

Appendix C. Design code calculations

C.1. Maximum allowable annual fatigue load

The design equation for the fatigue limit state is (DNV GL, 2018)

$$d_c \cdot \gamma_F \leq 1 \tag{C.1}$$

where d_c is a characteristic fatigue damage and γ_F is the fatigue safety factor. Let L denote the service life in years, and let $d_{c,\mathrm{yr}}$ denote the average, characteristic fatigue damage per year. The design equation may then be written

$$L \cdot d_{c,\mathrm{yr}} \cdot \gamma_F \leq 1 \tag{C.2}$$

Now, the average annual fatigue damage may be expressed as

$$d_{c,\mathrm{yr}} = \frac{\mathrm{E}[n_0 \cdot S^m]}{A_D} = \frac{\bar{Z}}{A_D} \tag{C.3}$$

where A_D is the intercept parameter of the S-N design curve and $\bar{Z} = \mathrm{E}[Z]$ is the expected annual fatigue load. Combining (C.2) and (C.3), the maximum allowable annual fatigue load becomes

$$\bar{Z} \leq \frac{A_D}{L \cdot \gamma_F} \tag{C.4}$$

Hence, with $L = 15$ [years], $\gamma_F = 8$ and $A_D = 6{\times}10^{10}$ (DNV GL, 2018), we get $\bar{Z} \leq 5{\times}10^8$ [MPa^3].

C.2. Correction for material loss

When corrosion is accounted for by means of a corrosion rate, representing the annual material loss, the effective chain diameter after k years is

$$\mathrm{d}_{\mathrm{k}}^{(\mathrm{crs})} = \mathrm{d}_0^{(\mathrm{crs})} - c_r \cdot k \tag{C.5}$$

where $\mathrm{d}_0^{(\mathrm{crs})}$ is the nominal diameter and c_r is the corrosion rate expressing the reduction in diameter per year. For a given tension range distribution, the annual fatigue load is inversely proportional to the cross section area raised to m (the S-N curve stress range effect). The expected fatigue load in the kth year is therefore related to the effective diameter by

$$\bar{Z}_k \propto \left(\frac{1}{\mathrm{d}_{\mathrm{k}}^{(\mathrm{crs})}} \right)^{2m} \tag{C.6}$$

Combining (C.5) and (C.6), a scaling factor for the expected effective fatigue load may thus be expressed as

$$\frac{\bar{Z}_k}{\bar{Z}_0} = \left(1 - \frac{c_r \cdot k}{\mathrm{d}_0^{(\mathrm{crs})}} \right)^{-2m} \tag{C.7}$$

where $\bar{Z}_0$ is the expected annual fatigue load calculated based on the nominal diameter.

Appendix D. Sensitivity measures

D.1. Sobol' indices

The Sobol' indices obtained for the global sensitivity analysis are briefly presented. Consider the output of a generic model, $Y = f(\boldsymbol{X})$, where $\boldsymbol{X} = (X_1, X_2, \ldots, X_M)$ is a random vector of size M. The Sobol' indices quantify the impact on the uncertainty of Y from the uncertainty of each of the components, X_i, over the entire range of possible outcomes. In the context of the present study, the model $f(\cdot)$ may be the fatigue damage in Eq. (9) or the limit state function in Eq. (17), and $\boldsymbol{X}$ contains the random variables in Table 2.

Assuming that the components in $\boldsymbol{X}$ are mutually independent, the first-order Sobol' index may be expressed as (Saltelli et al., 2008):

$$S_i = \frac{\mathrm{Var}_{X_i}(\mathrm{E}_{\boldsymbol{X}_{\sim i}}[Y|X_i])}{\mathrm{Var}(Y)} \tag{D.1}$$

where $\mathrm{Var}(\cdot)$ denotes variance and $\mathrm{E}[.]$ is the expectation. The subscript $\cdot_{X_i}$ means that the variance (or expectation) is taken over the range of possible outcomes for component X_i, whereas subscript $\cdot_{\boldsymbol{X}_{\sim i}}$ means that it is taken over the range of possible outcomes for all components except X_i. The first-order index quantifies the proportion of the uncertainty in Y that may be attributed to the uncertainty in X_i alone, and is a number between 0 and 1.

Similarly, the total-effect Sobol' index may be expressed as:

$$S_{Ti} = 1 - \frac{\mathrm{Var}_{\boldsymbol{X}_{\sim i}}(\mathrm{E}_{X_i}[Y|\boldsymbol{X}_{\sim i}])}{\mathrm{Var}(Y)} = \frac{\mathrm{E}_{\boldsymbol{X}_{\sim i}}(\mathrm{Var}_{X_i}[Y|\boldsymbol{X}_{\sim i}])}{\mathrm{Var}(Y)} \tag{D.2}$$

and quantifies the total contribution from uncertainty in X_i to the variance of Y, including interactions with other random variables. For a purely additive model, we have $S_{Ti} = S_i$ and $\sum_i S_i = 1$. The quantity $1 - \sum_i S_i$ may therefore be used to quantify the proportion of the variance that is caused by non-additive interactions in the model. Furthermore, zero total effect ($S_{Ti} = 0$) is a necessary and sufficient condition for X_i to be non-influential. Hence; given $S_{Ti} = 0$, the random variable X_i may be fixed to any value without affecting the variance of Y. Further details are found in e.g., Saltelli et al. (2008).

D.2. FORM-based sensitivity measures

The design point may also be expressed as $\boldsymbol{u}^* = \beta\boldsymbol{\alpha}$, where $\boldsymbol{\alpha} = (u_1^*/\beta, \ldots, u_M^*/\beta)$ is a vector containing directional cosines. It also represents the normal vector of the limit state surface at the design point, and it follows from the definition of the reliability index (β) that $\|\boldsymbol{\alpha}\| = \boldsymbol{\alpha}^T\boldsymbol{\alpha} = 1$, and $\beta = \boldsymbol{\alpha}^T\boldsymbol{u}^*$. Hence:

$$\left.\frac{\partial\beta}{\partial u_i}\right|_{\boldsymbol{u}=\boldsymbol{u}^*} = \alpha_i \tag{D.3}$$

which means that α_i is a local measure of the sensitivity of the reliability index to the uncertainty in U_i, evaluated at the design point. This sensitivity measure is referred to as the FORM *importance factors*, and is commonly presented in terms of the squared value, α_i^2, satisfying $\sum_i \alpha_i^2 = 1$. The factor α_i^2 describes the proportion of the variance of the linearized limit state function that is caused by the uncertainty in U_i (Madsen, 1988). When the random variables are independent in physical space, there is a one-to-one relation between U_i and X_i, and this interpretation of α_i^2 is valid also for the importance of X_i.

The *omission sensitivity factors* introduced by Madsen (Madsen, 1988) quantify the relative change in the reliability index if the random variable X_i is replaced by a fixed value. Specifically; for independent variables in physical space, the change in reliability index if X_i is replaced by its mean value is (Madsen, 1988):

$$\frac{\beta(X_i = \mu_{X_i})}{\beta} = \frac{1}{\sqrt{1-\alpha_i^2}} \tag{D.4}$$

References

Aksnes, V., Berthelsen, P.A., Fonseca, N.M.M.D.D., Reinholdtsen, S.-A., 2015. On the need for Calibration of numerical models of large floating units against experimental data. In: Proceedings of the Twenty-Fifth International Ocean and Polar Engineering Conference. International Society of Offshore and Polar Engineers, URL http://onepetro.org/ISOPEIOPEC/proceedings-pdf/ISOPE15/All-ISOPE15/ISOPE-I-15-264/1342795/isope-i-15-264.pdf/1.

Bury, K., 1975. Distribution of smallest log-normal and gamma extremes. Stat. Hefte 16 (2), 105–114. http://dx.doi.org/10.1007/BF02922919, URL http://link.springer.com/10.1007/BF02922919.

Bury, K., 1999. Statistical Distributions in Engineering. Cambridge University Press, http://dx.doi.org/10.1017/CBO9781139175081, URL https://www.cambridge.org/core/product/identifier/9781139175081/type/book.

DNV GL, 2018. Offshore standard - Position mooring (DNVGL-OS-E301), Edition July 2018.

Fernández, J., Arredondo, A., Storesund, W., González, J.J., 2019. Influence of the mean load on the fatigue performance of mooring chains. In: Proceedings of the Annual Offshore Technology Conference. (OTC-29621-MS), http://dx.doi.org/10.4043/29621-MS.

Fontaine, E., Kilner, A., Carra, C., Washington, D., Ma, K.T., Phadke, A., Laskowski, D., Kusinski, G., 2014. Industry survey of past failures, pre-emptive replacements and reported degradations for mooring systems of floating production units. In: Offshore Technology Conference. (OTC-25273-MS), Offshore Technology Conference, Houston, Texas, http://dx.doi.org/10.4043/25273-MS.

Gabrielsen, Ø., Larsen, K., Dalane, O., Lie, H.B., Reinholdtsen, S.-A., 2019. Mean load impact on mooring chain fatigue capacity: Lessons learned from full scale fatigue testing of used chains. In: Proceedings of the ASME 2019 38th International Conference on Ocean, Offshore and Arctic Engineering. (OMAE2019-95083), http://dx.doi.org/10.1115/OMAE2019-95083.

Gabrielsen, Ø., Reinholdtsen, S.-A., Skallerud, B., Haagensen, P.J., Andersen, M., Kane, P.-A., 2022. Fatigue capacity of used mooring chain - results from full scale fatigue testing at different mean loads. In: Proceedings of the ASME 2022 41st International Conference on Ocean, Offshore and Arctic Engineering. (OMAE2022-79649), Hamburg, Germany.

Gelman, A., Hill, J., 2007. Data Analysis using Regression and Multilevel/Hierarchical Models. In: Analytical Methods for Social Research, Cambridge University Press, Cambridge, http://dx.doi.org/10.1017/CBO9780511790942.

ISO 19901-7, 2013. Petroleum and Natural Gas Industries - Specific Requirements for Offshore Structures - Part 7: Stationkeeping Systems for Floating Offshore Structures and Mobile Offshore Units, second ed. International Organization for Standardization.

Jacques, J., Lavergne, C., Devictor, N., 2006. Sensitivity analysis in presence of model uncertainty and correlated inputs. Reliab. Eng. Syst. Saf. 91 (10–11), 1126–1134. http://dx.doi.org/10.1016/j.ress.2005.11.047, URL https://linkinghub.elsevier.com/retrieve/pii/S0951832005002231.

JCSS, 2011. Probabilistic Model Code. Part 3: Resistance Models. Section 3.12 Fatigue. Joint Committee on Structural Safety.

Kapur, J.N., 1989. Maximum-Entropy Models in Science and Engineering. John Wiley & Sons, New York.

Kvitrud, A., 2014. Lessons learned from norwegian mooring line failures 2010–2013. In: Proceedings of the ASME 2014 33rd International Conference on Ocean, Offshore and Arctic Engineering. pp. 1–10. http://dx.doi.org/10.1115/OMAE2014-23095.

Lardier, J., Moan, T., Gao, Z., 2008. Fatigue reliability of catenary mooring lines under corrosion effect. In: Proceedings of the ASME 2008 27th International Conference on Offshore Mechanics and Arctic Engineering. Vol. 2. (OMAE2008-57360), pp. 351–358. http://dx.doi.org/10.1115/OMAE2008-57360.

Larsen, K., Mathisen, J., 1996. Reliability-based fatigue analysis of mooring lines. In: Proceedings of the 15th International Conference on Ocean, Offshore Mechanics and Arctic Engineering.

Lemaire, M., 2009. Structural Reliability. ISTE, London, UK, http://dx.doi.org/10.1002/9780470611708, URL http://doi.wiley.com/10.1002/9780470611708.

Lone, E.N., Sauder, T., Larsen, K., Leira, B.J., 2021. Fatigue assessment of mooring chain considering the effects of mean load and corrosion. In: Proceedings of the ASME 2021 40th International Conference on Ocean, Offshore and Arctic Engineering. (OMAE2021-62775), http://dx.doi.org/10.1115/OMAE2021-62775, Virtual.

Lone, E.N., Sauder, T., Larsen, K., Leira, B.J., 2022. Probabilistic fatigue model for design and life extension of mooring chains, including mean load and corrosion effects. Ocean Eng. 245, 110396. http://dx.doi.org/10.1016/j.oceaneng.2021.110396, URL https://linkinghub.elsevier.com/retrieve/pii/S0029801821016863.

Lotsberg, I., 2016. Fatigue Design of Marine Structures. Cambrige University Press, http://dx.doi.org/10.1017/CBO9781316343982.

Ma, K.-t., Gabrielsen, Ø., Li, Z., Baker, D., Yao, A., Vargas, P., Luo, M., Izadparast, A., Arredondo, A., Zhu, L., Sverdlova, N., Høgsæt, I.S., 2019. Fatigue tests on corroded mooring chains retrieved from various fields in offshore west Africa and the North Sea. In: Proceedings of the ASME 2019 38th International Conference on Ocean, Offshore and Arctic Engineering. (OMAE2019-95618).

Ma, K.-t., Shu, H., Smedley, P., L'Hostis, D., Duggal, A., 2013. A historical review on integrity issues of permanent mooring systems. In: Offshore Technology Conference. (OTS-24025-MS), Offshore Technology Conference, Houston, Texas, USA, http://dx.doi.org/10.4043/24025-MS.

Madsen, H.O., 1988. Omission sensitivity factors. Struct. Saf. 5 (1), 35–45. http://dx.doi.org/10.1016/0167-4730(88)90004-5.

Martinez Perez, I., Bastid, P., Constantinescu, A., Venugopal, V., 2018. Multiaxial fatigue analysis of mooring chain links under tension loading: Influence of mean load and simplified assessment. In: Proceedings of the ASME 2018 37th International Conference on Ocean, Offshore and Arctic Engineering. Vol. 3. (OMAE2018-77552), pp. 1–11. http://dx.doi.org/10.1115/OMAE2018-77552.

Martinez Perez, I., Constantinescu, A., Bastid, P., Zhang, Y.H., Venugopal, V., 2019. Computational fatigue assessment of mooring chains under tension loading. Eng. Fail. Anal. 106 (June), 104043. http://dx.doi.org/10.1016/j.engfailanal.2019.06.073.

Mathisen, J., Hørte, T., 2005. Calibration of a fatigue limit state for mooring lines. In: International Conference on Computational Methods in Marine Engineering MARINE 2005. Barcelona.

Mathisen, J., Hørte, T., Moe, V., Lian, W., 1999. Joint Industry Project – DEEPMOOR – Design Methods for Deep water Mooring Systems, Calibration of a Fatigue Limit States. DNV Report, (97-3583, Rev. 03), Det Norske Veritas.

Melchers, R., Beck, A.T., 2018. Structural Reliability Analysis and Prediction, third ed. John Wiley & Sons, Inc. Hoboken, NJ.

Mendoza, J., Haagensen, P.J., Köhler, J., 2022. Analysis of fatigue test data of retrieved mooring chain links subject to pitting corrosion. Mar. Struct. 81, 103119. http://dx.doi.org/10.1016/j.marstruc.2021.103119, URL https://linkinghub.elsevier.com/retrieve/pii/S0951833921001702.

Saltelli, A., Annoni, P., Azzini, I., Campolongo, F., Ratto, M., Tarantola, S., 2010. Variance based sensitivity analysis of model output. Design and estimator for the total sensitivity index. Comput. Phys. Comm. 181 (2), 259–270. http://dx.doi.org/10.1016/j.cpc.2009.09.018, URL https://linkinghub.elsevier.com/retrieve/pii/S0010465509003087.

Saltelli, A., Ratto, M., Andres, T., Campolongo, F., Cariboni, J., Gatelli, D., Saisana, M., Tarantola, S., 2008. Global sensitivity analysis. In: The Primer. John Wiley & Sons, Ltd, Chichester, UK, http://dx.doi.org/10.1002/9780470725184, URL http://doi.wiley.com/10.1002/9780470725184.

Sauder, T., 2021. Empirical estimation of low-frequency nonlinear hydrodynamic loads on moored structures. Appl. Ocean Res. 117, 102895. http://dx.doi.org/10.1016/J.APOR.2021.102895, URL https://linkinghub.elsevier.com/retrieve/pii/S0141118721003667.

Sauder, T., Mainçon, P., Lone, E., Leira, B.J., 2022. Estimation of top tensions in mooring lines by sensor fusion. Marine Structures (in press).

Sobol', I.M., 1993. Sensitivity estimates for nonlinear mathematical models. Math. Model. Comput. Exp. 1 (4), 407–414.

Straub, D., Schneider, R., Bismut, E., Kim, H.-J., 2020. Reliability analysis of deteriorating structural systems. Struct. Saf. 82, 101877. http://dx.doi.org/10.1016/j.strusafe.2019.101877, URL https://linkinghub.elsevier.com/retrieve/pii/S0167473018303254.

Wang, S., Zhang, X.Y., Kwan, T., Ma, K., Li, Z., Baker, D.A., Izadparast, A., Farrow, G.H., Potts, A.E., Nair, A., Prabhu, M.L., Vargas, P.M., Perez, I.M., Luo, M., Fontaine, E., 2019. Assessing fatigue life of corroded mooring chains through advanced analysis. In: Offshore Technology Conference. (OTC-24994), Offshore Technology Conference, Houston, Texas, p. 25. http://dx.doi.org/10.4043/29449-MS.

Wirsching, P.H., 1984. Fatigue reliability for offshore structures. J. Struct. Eng. 110 (10), 2340–2356. http://dx.doi.org/10.1061/(ASCE)0733-9445(1984)110:10(2340).

Wirsching, P.H., Chen, Y.N., 1988. Considerations of probability-based fatigue design for marine structures. Mar. Struct. 1 (1), 23–45. http://dx.doi.org/10.1016/0951-8339(88)90009-3.

Zarandi, E.P., Skallerud, B.H., 2020. Experimental and numerical study of mooring chain residual stresses and implications for fatigue life. Int. J. Fatigue http://dx.doi.org/10.1016/j.ijfatigue.2020.105530.

Zhang, Y., Smedley, P., 2019. Fatigue performance of high strength and large diameter mooring chain in seawater. In: Proceedings of the ASME 2019 38th International Conference on Ocean, Offshore and Arctic Engineering. (OMAE2019-95984), http://dx.doi.org/10.1115/OMAE2019-95984.